Ms. No. JCAT-13-373

Bimodal Cesium Hydrogen Salts of 12-Tungstosilicic Acid, $Cs_xH_{4-x}SiW_{12}O_{40}$, as Highly Active Solid Acid Catalysts for Transesterification of Glycerol Tributyrate with Methanol

Yukari Iwase,[a] Shogo Sano,[b] Lina Mahardiani,[b] Ryu Abe,[a] Yuichi Kamiya*[c]

[a] Department of Energy and Hydrocarbon Chemistry, Graduate School of Engineering, Kyoto University, Katsura, Nishikyo-ku, Kyoto 615-8510, Japan

[b] Graduate School of Environmental Science, Hokkaido University, Nishi 5, Kita 10, Kita-ku, Sapporo 060-0810, Japan

[c] Research Faculty of Environmental Earth Science, Hokkaido University, Nishi 5, Kita 10, Kita-ku, Sapporo 060-0810, Japan

*Corresponding author

Yuichi Kamiya

E-mail: kamiya@ees.hokudai.ac.jp, Tel/Fax:+81-11-706-2217

ABSTRACT

Bimodal $Cs_xH_{4-x}[SiW_{12}O_{40}]$ (**Cs*x*-bimodal**) with mesopores interconnected with micropores were synthesized from microporous $Cs_xH_{4-x}[SiW_{12}O_{40}]$ (**Cs*x*-micro**) with x = 1.0–2.5, which were prepared in advance by titrating an aqueous solution of $H_4[SiW_{12}O_{40}]$ with an aqueous solution of Cs_2CO_3, followed by treatment in refluxing ethanol to mainly dissolve the $H_4[SiW_{12}O_{40}]$ in the particles. Mesopore size distributions and their pore volumes changed depending on x in **Cs*x*-micro**. Microporous **Cs2.5-micro** transformed into bimodal **Cs2.5-bimodal** with mesopores having average diameters of 3.7 nm and large mesopore volumes. Although **Cs2.5-bimodal** exhibited only low catalytic activity for the decomposition of isopropyl acetate, post-treatment in H_2SO_4 enhanced the catalytic activity due to substitution of the Cs^+ ions on the surface with H^+. H_2SO_4-treated **Cs*x*-bimodal** showed high activity towards transesterification of glyceryl tributyrate with methanol due to its strong acid strength and mesoporosity.

Keywords: Heteropolyacid; Mesopore, Bimodal; Biodiesel; Solid acid; Dissolution

1. Introduction

Bimodal porous materials having ordered micropores and ordered mesopores that are interconnected can be used as catalysts for reactions involving bulky reactants and products [1-17]. Bimodal solid catalysts are expected to show high catalytic activities because they have large numbers of active sites due to high surface areas arising from the micropores and because of fast diffusion of the reactants in the interconnected mesopores. In addition, the bimodal pores can suppress catalyst deactivation due to coking in reactions involving hydrocarbon conversion because of the smooth release of the products from the area around the active site through the interconnected mesopores [8, 18-20]. Thus, rational design of hierarchical pore structures and the active sites in the catalysts is important for developing highly active, selective, and highly durable solid catalysts.

There has been extensive research to prepare bimodal solid catalysts in crystalline microporous aluminosilicate zeolites with ordered mesopores. Methods for fabricating such bimodal zeolites involve (i) forming mesopores in the zeolite particles concurrently with crystallization of the zeolite framework [21-25] and (ii) forming mesopores that pass through the zeolite crystallite by dissolving a part of the zeolite crystallite prepared in advance [26-29]. In the former method, hard (e.g., mesoporous carbons [21], carbon nanoparticles [24], and carbon nanotubes [23]) and soft (e.g., micelles formed with

surfactants [22]) materials with ordered mesostructures are used as templates to create mesopores. Zeolites are crystallized inside the nanospaces of the template or around the template, followed by removal of the template to form the mesopores.

On the other hand, a typical example of the latter method is to heat zeolites in a strong alkaline solution to dissolve a part of the zeolite crystallites [26-29]. Ogura et al. have reported that thermal treatment of MFI zeolites in aqueous NaOH solutions results in the selective dissolution of siliceous species in the zeolite to form mesopores with uniform sizes [27, 30]. The treatment doubles the diffusion rate of benzene inside the catalyst particle, and the obtained bimodal MFI zeolite shows higher catalytic activity for cumene cracking than the original microporous one does [27]. Although bimodal zeolites with ordered mesopores are useful solid catalysts, their uses as solid acid catalysts are limited because their acid strengths are relatively weak. Thus, there has been strong interest towards the development of bimodal solids with strong acid sites, other than zeolites, in order to expand the range of their possible applications to challenging acid-catalyzed reactions.

Keggin-type heteropolyacids, $H_n[XY_{12}O_{40}]$, are molecular metal oxide clusters with discrete molecular structures [31-33]. Keggin-type heteropolyacids with tungsten as addenda atoms, including $H_3[PW_{12}O_{40}]$ and $H_4[SiW_{12}O_{40}]$, have strong Brønsted acid sites, which are stronger than those of

common aluminosilicate zeolites and are comparable to those of sulfated zirconia [34-36]. In fact, initial heats of ammonia adsorption for $H_3[PW_{12}O_{40}]$ and $H_4[SiW_{12}O_{40}]$ are 195 and 175 kJ mol^{-1}, respectively [37, 38], whereas those for MFI zeolites and amorphous silica-alumina are 150 and 145 kJ mol^{-1}, respectively [35, 39]. Thus, heteropolyacids are classified as superacids [31]. Moreover, the superacidity of Keggin-type heteropolyacids has been demonstrated on the basis of solid-state ^{31}P MAS NMR of trymethyl phosphine oxide (TMPO) adsorbed on them [40, 41].

Although solid-state Keggin-type heteropolyacids are non-porous and thus have small surface areas (< 15 m^2 g^{-1}), substitution of H^+ with Cs^+ leads to an increase in the surface area and to the formation of pores. The surface area and pore structure change depending on the degree of the substitution of H^+ [42-45]. Thus far, the syntheses, structural analyses, and catalytic activity of neutral and acidic Cs^+ salts of $H_3[PW_{12}O_{40}]$ have been extensively investigated [31, 44, 46-50]. It has been reported that $Cs_{2.1}H_{0.9}[PW_{12}O_{40}]$ is microporous and has no mesopores and that it acts as a size-selective catalyst for acid-catalyzed reactions [44, 47-49]. Since $Cs_{2.1}H_{0.9}[PW_{12}O_{40}]$ crystallites themselves have no micropores [47], their micropores form due to crystallographic mismatching between the facets of the crystallites [47].

On the other hand, the pores of $Cs_xH_{3-x}[PW_{12}O_{40}]$ with $x \geq 2.3$ show bimodal distributions, ranging

from microporous to mesoporous, and the interparticle spaces form the mesopores [51]. $Cs_xH_{3-x}[PW_{12}O_{40}]$ with $x = 2.5$ has a large surface area and consequently the largest number of surface acid sites among $Cs_xH_{3-x}[PW_{12}O_{40}]$ [52]. Due to the large number of surface acid sites, bimodal pores, and strong acid strengths, the Cs salts exhibit extremely high catalytic activities for various acid-catalyzed reactions involving bulky reactants [52-54].

Although the molecular structure of $H_4[SiW_{12}O_{40}]$ is similar to that of $H_3[PW_{12}O_{40}]$ and the major difference between $H_4[SiW_{12}O_{40}]$ and $H_3[PW_{12}O_{40}]$ is the electronic charges of the heteropoly anions, which are –4 and –3, respectively, the mechanisms for the formation of the pores and for the changes in the pore structure on the degree of substitution of H^+ with Cs^+ in $H_4[SiW_{12}O_{40}]$ are quite different from those of $H_3[PW_{12}O_{40}]$. In the crystal of the Cs salts of $H_4[SiW_{12}O_{40}]$ ($Cs_xH_{4-x}[SiW_{12}O_{40}]$), heteropoly anions ($[SiW_{12}O_{40}]^{4-}$) are packed in a body-centered cubic (bcc) cell and cations exist between anions. $Cs_xH_{4-x}[SiW_{12}O_{40}]$ form microporous solids with low external surface areas (less than 4% of the total surface area) and do not have mesopores, regardless of the substitution degree of H^+ [45]. Microporous $Cs_3H[SiW_{12}O_{40}]$, which has the highest surface area among $Cs_xH_{4-x}[SiW_{12}O_{40}]$, acts as a size-selective catalyst towards acid-catalyzed reactions in the liquid phase due to its uniform micropores and small external surface area [45]. The micropores in $Cs_3H[SiW_{12}O_{40}]$ originate from defects in the heteropoly

anions, which form to avoid mismatches in the $Cs^+/[SiW_{12}O_{40}]^{4-}$ ratio required for charge balance (= 4/1) and for a bcc structure (= 3/1) [45, 55, 56]. If the ordered mesopores that are interconnected with the micropores are present in microporous $Cs_xH_{4-x}[SiW_{12}O_{40}]$, the resulting bimodal Cs salts should show high catalytic activity for acid-catalyzed reactions involving bulky reactants. In other words, bimodal porosity will expand the possible applications of $Cs_xH_{4-x}[SiW_{12}O_{40}]$ as a solid acid catalyst.

In the present study, we synthesized bimodal $Cs_xH_{4-x}[SiW_{12}O_{40}]$ with micropores and interconnected mesopores by treating microporous $Cs_xH_{4-x}[SiW_{12}O_{40}]$ with x = 1.0–2.5 in refluxing ethanol. A formation mechanism of the mesopores is discussed on the basis of the dissolution rate of microporous $Cs_xH_{4-x}[SiW_{12}O_{40}]$ during treatment and structural and compositional analyses of the Cs salts before and after treatment. Furthermore, we investigated the post-treatment of the resulting bimodal $Cs_xH_{4-x}[SiW_{12}O_{40}]$ in sulfuric acid to increase the number of acid sites and consequently to improve the catalytic activity towards acid-catalyzed reactions. Finally, we conducted transesterification of glycerol tributyrate with methanol over the sulfuric acid-treated bimodal $Cs_xH_{4-x}[SiW_{12}O_{40}]$ to demonstrate the advantage of mesopores in catalysts for reactions involving bulky reactants.

2. Experimental

2.1. Materials

Dodecatungstosilicic acid ($H_4[SiW_{12}O_{40}]\cdot nH_2O$) was supplied by Nippon Inorganic Color and Chemical Co. After $H_4[SiW_{12}O_{40}]\cdot nH_2O$ was recrystallized from water several times, it was dried in a vacuum at 338 K to obtain $H_4[SiW_{12}O_{40}]\cdot 8H_2O$.

Cesium carbonate, ethanol, propanol, isopropyl acetate, *n*-hexyl ether, 1,3,5-triisopropyl benzene, *n*-decane, and sulfuric acid were obtained from Wako Pure Chem. Ind., Ltd. and used as received. Glycerol tributyrate ($C_{15}H_{26}O_6$, Tokyo Chem. Ind. Co., Ltd.) and methanol (Wako Pure Chem. Ind., Ltd) were treated with anion-exchange resin (Amberlite IRA400J CL, Organo Co.) and cation-exchange resin (Amberlite 200C, Organo Co.) to remove both acidic and basic impurities before use.

Zeolites including H-Y (JRC-Z-HY5.6), H-β (JRC-Z-HB25H), and H-ZSM-5 (JRC-Z5-25H) and silica-alumina (JRC-SAH-1) were supplied from the Catalysis Society of Japan as reference catalysts. $Cs_{2.5}H_{0.5}[PW_{12}O_{40}]$ was prepared by using a previously reported procedure [50].

2.2. Synthesis

2.2.1. Microporous $Cs_xH_{4-x}[SiW_{12}O_{40}]$ (**Cs*x*-micro**)

$Cs_xH_{4-x}[SiW_{12}O_{40}]$ with different Cs contents (x = 1.0, 1.5, 2.0, 2.5, 3.0, 3.5, and 4.0) were prepared

by titrating an aqueous solution of $H_4[SiW_{12}O_{40}]$ (0.08 mol dm^{-3}, 20 cm^3) with an aqueous solution of Cs_2CO_3 (0.10 mol dm^{-3}) at room temperature while vigorously stirring [45]. *x* was adjusted by changing the amount of the Cs_2CO_3 solution added, which was carefully controlled by using an automatic syringe pump: first, 2 cm^3 was added at a rate of 0.033 cm^3 min^{-1}, and then the remaining solution was added at a rate of 0.2 cm^3 min^{-1}. The resulting colloidal solution was allowed to stand for 48 h at room temperature, and then the solvent was evaporated at 313 K to obtain $Cs_xH_{4-x}[SiW_{12}O_{40}]$ as a white solid. After grinding the solid, it was dried in a vacuum at room temperature. The resulting solids are denoted as **Cs*x*-micro**, in which *x* represents the Cs content.

2.2.2. Bimodal $Cs_xH_{4-x}[SiW_{12}O_{40}]$ (**Cs*x*-bimodal**)

Cs*x*-micro (2 g) was added to ethanol (30 cm^3), and the suspension was refluxed at 347 K for 4 h with stirring. The remaining solid was collected on a membrane filter (ϕ 0.2 μm) and washed three times with ethanol. After the solid was dried at room temperature, it was weighed to estimate the dissolution rate (eq. 1).

$$\text{Disolution rate of } \mathbf{Cs}x\text{-}\mathbf{micro}\ (\%) = \frac{2 - \text{Weight of the solid remaining after the treatment [g]}}{\text{Initial weight of the solid [2 g]}} \times 100 \quad \text{(eq. 1)}$$

The solid was calcined in air at 523 K for 4 h. The resulting solids are denoted as **Cs*x*-bimodal**, in which *x* represents the Cs content in the original **Cs*x*-micro**.

To investigate the influence of the solvent, **Cs2.5-micro** was treated in water and 1-propanol in a similar manner to that in ethanol.

2.2.3. Post-treatment of **Cs2.5-bimodal** in sulfuric acid

Cs2.5-bimodal (1.0 g) was added to 25% sulfuric acid (15 cm^3), and the suspension was heated at 353 K for 2 h with stirring. The solid was collected on a membrane filter (ϕ 0.2 μm) and washed with water. The solid was dried under ambient conditions for 24 h and then calcined in air at 523 K for 4 h. The resulting solid is denoted as **Cs2.5-bimodal(H_2SO_4)**.

2.3. Characterization

Nitrogen adsorption-desorption isotherms were measured at 77 K on a Belsorp-mini instrument (BEL Japan Inc.) after pretreatment of the samples at 473 K in a flow of N_2 for 0.5 h. Mesopore-size distributions and mesopore volumes were determined by using the Dollimore-Heal (DH) method on an N_2

desorption isotherm. The micropore-size distribution was determined by using the Saito-Foley method [57] on an Ar adsorption isotherm at 87 K measured with an automatic apparatus (Belsorp 28SA, BEL Japan Inc.). Before measurement, the sample was pretreated at 473 K in a vacuum for 10 h.

Powder X-ray diffraction (XRD) was performed using an X-ray diffractometer (Rigaku Mini Flex) with Cu Kα radiation (λ = 0.154 nm). Crystallite size was determined by using Scherrer's equation with a diffraction line at 2θ = 25 ~ 26°. Elemental analyses of the samples were performed on an atomic absorption spectrometer (Hitachi A-2000) and an inductively coupled plasma-atomic emission spectrometer (Shimadzu ICPS-7000) for Cs and W, respectively. Scanning electron microscopy (SEM) images were obtained on an FE-SEM (Hitach, S-4800).

Temperature-programmed desorption of ammonia (NH_3-TPD) was carried out by using a multi-task TPD system (BEL Japan Inc.) equipped with a quadrupole mass spectrometer. After pretreatment at 473 K for 1 h in a flow of He (50 cm^3 min^{-1}), the catalyst was exposed to NH_3 at 13 kPa and 373 K for 0.5 h, and then the excess NH_3 was removed in a He flow at 373 K for 0.5 h. The temperature of the catalyst was increased at a rate of 10 K min^{-1} to 1073 K, and the desorbed gas was monitored at m/z = 16.

2.4. Catalytic reaction

Decomposition of isopropyl acetate was performed in a batch type reactor at 373 K. After the catalyst (0.1 g) was pretreated in a flow of N_2 at 473 K for 0.5 h, *n*-decane (solvent, 28 cm^3), 1,3,5-triisopropyl benzene (internal standard, 4 mmol) and isopropyl acetate (8 mmol) were introduced into the reactor. Then, the reactor was heated at 373 K while the solution was stirred. Samples (*ca*. 0.1 cm^3) were taken from the reaction solution at 0.5, 1, 1.5, and 2 h. The catalyst in the sample solution was immediately separated by centrifugation (9000 rpm and 10 min), and the supernatant was analyzed by using a gas chromatograph (Shimadzu, GC-2010) equipped with a capillary column (Neutrabond-1, 60 m × 0.25 mm, GL Science Inc.) and a flame ionization detector (FID-GC). The conversion was defined as eq. 2.

$$\text{Conversion (\%)} = \frac{\text{[Initial amount of isopropyl acetate]-[Amount of isopropyl actetate at } x \text{ h]}}{\text{[Initial amount of isopropyl acetate]}} \times 100 \qquad \text{(eq. 2)}$$

No product other than acetic acid formed in the liquid phase, and propylene separated from the solution.

Transesterification of glyceryl tributyrate with methanol was also performed in the batch type reactor at 333 K. The catalyst (0.2 g) was pretreated in a flow of N_2 at 473 K for 0.5 h. Methanol (300 mmol), *n*-hexyl ether (internal standard, 2.5 mmol), and glyceryl tributyrate (10 mmol) were introduced into the

reactor, and then the reactor was heated at 333 K while the solution was stirred. After 24 h, the catalyst was separated by centrifugation (9000 rpm and 10 min), and the supernatant was analyzed by using a gas chromatograph (Shimadzu, GC-14B) equipped with a capillary column (Neutrabond-1, 60 m × 0.25 mm) and a flame ionization detector (FID-GC). Amberlyst-15 (Organo Co.) was pretreated at 373 K to prevent catalyst decomposition. The yield of methyl butyrate was defined as shown in eq. 3.

$$\text{Yield (\%)} = \frac{[\text{Amount of formed methyl butyrate}]}{[\text{Initial amount of glycerol tributyrate}] \times 3} \times 100 \qquad \text{(eq. 3)}$$

3. Results and discussion

3.1. Formation of mesopores by treatment of **Cs*x*-micro** in refluxing ethanol

Figure 1 shows N_2 adsorption–desorption isotherms for **Cs*x*-micro** and **Cs*x*-bimodal**. In the case of **Cs*x*-micro**, a type I isotherm was observed regardless of *x*, indicating that these were microporous materials [45]. The amount of N_2 uptake for **Cs*x*-micro** increased with an increase in *x* to 3.0 and 3.5 (Figures 1e and f, circles). As a result, **Cs3.0-micro** (192 $m^2 g^{-1}$) and **Cs3.5-micro** (187 $m^2 g^{-1}$) had the largest surface areas among **Cs*x*-micro** (Figure S1). For **Cs*x*-micro** with *x* = 1.0–2.5, the isotherms were dramatically changed by treatment in refluxing ethanol, and those of the corresponding

Cs*x*-bimodal were type IV isotherms. The results indicate that the treatment causes the formation of mesopores in **Cs*x*-bimodal** with x = 1.0–2.5 (Figure S2). In the isotherm for **Cs2.5-bimodal**, a clear hysteresis loop was observed. In addition, a steep increase in the N_2 adsorption amount at low pressures remained even after treatment, indicating that the micropores were preserved. The surface areas were slightly increased for the samples with x = 1.0–2.5 by the treatment. In contrast, no change was observed in the isotherms for the materials with $x \geq 3$.

Figure 2 shows pore-size distributions of the micropores and mesopores in **Cs2.5-micro** and **Cs2.5-bimodal**. In the micropore-size distribution for **Cs2.5-micro** (solid line), an intense peak at 0.52 nm (**Micropore α**) and a shoulder at around 0.62 nm (**Micropore β**) were observed. It has been reported that cesium hydrogen salts of 12-tungstosilicic acid, like $Cs_{3.0}H_{0.3}[SiW_{12}O_{40}]_{0.83}\cdot 3H_2O$ [56] and $Cs_3H[SiW_{12}O_{40}]$ [45], have anion ($[SiW_{12}O_{40}]^{4-}$) vacancies in the crystal lattice to compensate for the excess negative charges and that these vacancies form the micropores [45]. After the treatment in refluxing ethanol, **Micropore β** was preserved, whereas **Micropore α** partially collapsed. The changes in the micropore-size distributions due to the treatment will be discussed later.

In contrast to the micropore-size distributions, the mesopore size ones were completely different after the treatment. Although for **Cs2.5-micro**, there was only a small peak in the mesopore region, a

clear intense peak at 3.7 nm appeared for **Cs2.5-bimodal**. The mesopore volume of **Cs2.5-bimodal** was 71 $mm^3\ g^{-1}$. **Cs2.5-bimodal** was thermally stable in air up to 723 K, which was confirmed from XRD patterns and N_2 adsorption–desorption isotherms. It seems that the mesopore volume per unit weight for **Cs2.5-bimodal** is not large in comparison with that of mesoporous silica, such as MCM-41 (> 700 $mm^3\ g^{-1}$) [58]. However, if the heavy formula weight of the heteropolyacid is taken into account ($FW_{Cs3H[SiW2O40]}$ = 3273 and FW_{SiO2} = 60), it can be concluded that that **Cs2.5-bimodal** is highly porous.

3.2. Formation mechanism of mesopores by the treatment of **Cs*x*-micro** in refluxing ethanol

The volumes of the mesopores in **Cs*x*-micro** and **Cs*x*-bimodal** estimated from N_2 desorption isotherms are compared in Figure 3. **Cs*x*-micro** with $x \leq 2.5$ transformed into **Cs*x*-bimodal** with large mesopore volumes, but there were no or only little changes for the materials with x = 3.5 and 4.

Acid-form Keggin-type heteropolyacids, like $H_4[SiW_{12}O_{40}]$, are usually highly soluble in water and polar organic solvents, including lower alcohols [31]. On the other hand, salts of Keggin-type heteropolyacids with large monovalent cations, such as Cs^+, have low solubility in those solvents [53]. Thus, we believe that the mesopores form by dissolution of a part of **Cs*x*-micro** in ethanol. Therefore, we determined the dissolution rate of **Cs*x*-micro** during treatment in ethanol. There was a distinct

correlation between the dissolution rate and *x* in **Cs*x*-micro**, as shown in Figure 4. Although $H_4[SiW_{12}O_{40}]$ completely dissolved in ethanol under the present conditions (data not shown), the Cs salts were less soluble. However, 61% of **Cs1.0-micro** was soluble in ethanol. The dissolution rate monotonically decreased with an increase in *x*. It is noted that **Cs3.5-micro** and **Cs4.0-micro**, both of which did not become bimodal Cs salts, were basically insoluble in ethanol under the present conditions.

The Cs/polyanion ratio (= Cs/12W) in the materials before (**Cs*x*-micro**) and after (**Cs*x*-bimodal**) the treatment gave valuable information about the component that dissolved during the treatment. In Figure 5, Cs/polyanion ratios for **Cs*x*-micro** and **Cs*x*-bimodal** are plotted as a function of *x*. The dashed line in the figure represents Cs/polyanion = *x*. The Cs/polyanion ratios for **Cs*x*-bimodal** were higher than those for the corresponding **Cs*x*-micro** for *x* = 1.0–2.5. For example, the Cs/polyanion ratio increased from 2.46 for **Cs2.5-micro** to 2.95 for **Cs2.5-bimodal**. The treatment caused a larger difference in the Cs/polyanion ratio for the materials with low *x* than it did for those with large *x*. The results clearly indicate that the part of **Cs*x*-micro** with low *x* dissolved into ethanol during the treatment. In the case of **Cs2.5-micro**, we estimated from the Cs/polyanion ratio and dissolution rate that the dissolving part of **Cs*x*-micro** had *x* = 0.65. In contrast, there was no change in the Cs/polyanion ratio for **Cs3.5-micro** and **Cs4.0-micro** upon the treatment due to no dissolution.

Figure 6 shows XRD patterns for **Cs*x*-micro** and **Cs*x*-bimodal**, and the XRD pattern for $H_4[SiW_{12}O_{40}]$ (**Cs0.0**) is included as a reference. All diffraction lines for **Cs3.5-micro** and **Cs4.0-micro** were assigned to a cubic structure, in which heteropoly anions are packed in a bcc cell. The lattice constant (*a*) for **Cs4.0-micro** was 1.177 nm, and this cubic phase is referred to as phase C. The XRD pattern for $H_4[SiW_{12}O_{40}]$ (**Cs0.0**) was also assigned to a cubic structure similar to **Cs4.0-micro**, but *a* was 1.212 nm (phase A). The large value of *a* for phase A is due to occupation of the cation sites with hydrated protons ($(H_2O)_nH^+$), which are larger than Cs^+. For **Cs*x*-micro** with x = 1.5–2.5, diffraction lines were broad, and the diffraction angles near $2\theta = 26°$ were between those of phase C ($2\theta = 26.20°$) and those of phase A ($2\theta = 25.40°$). As will be discussed later, **Cs*x*-micro** with x = 1.5–2.5 were composed of three phases (phase A, B, and C) and the value of *a* for phase B was between those for phases A and C. In phase B, the cation sites were occupied with Cs^+ and hydrated H^+. In the XRD pattern for **Cs1.0-micro**, two sets of the cubic XRD patterns consistent with phases A and B were observed.

After treating **Cs1.0-micro** in ethanol, phase A ($H_4[SiW_{12}O_{40}]$) completely disappeared, and only the XRD pattern for phase B with a = 1.187 nm was observed. For **Cs*x*-bimodal** with x = 1.5–2.5, the diffraction lines became sharp after the treatment. In addition, the skirts of the diffraction lines

broadened toward lower 2θ in **Cs*x*-micro** disappeared after the treatment. These results support the fact that $H_4[SiW_{12}O_{40}]$ and/or $Cs_xH_{4-x}[SiW_{12}O_{40}]$ with low *x* dissolved in ethanol and that $Cs_xH_{4-x}[SiW_{12}O_{40}]$ with high *x* did not. On the other hand, the XRD patterns for **Cs3.5-bimodal** and **Cs4.0-bimodal** did not change at all.

Dissolution of a part of **Cs*x*-micro** upon treatment was directly observed by using SEM (Figure 7). In an SEM micrograph for **Cs2.5-micro** (Figure 7a), fine particles (primary particle) with a size of ca. 10 nm were observed. The fine particles tightly aggregated to form secondary particles, eliminating any interstitial voids between the fine particles. The shape of the secondary particles and the size of the fine particles for **Cs2.5-bimodal** were quite similar to those for **Cs2.5-micro**. However, it appeared that some fine particles had fallen off the secondary particles forming interstitial voids in the secondary particles. The aperture sizes of the interstitial voids were less than 10 nm, which roughly agreed with the mesopore size estimated from the N_2 adsorption-desorption isotherm, indicating that the interstitial voids were mesopores.

To elucidate the formation mechanism of the mesopores, the formation process and microstructure of **Cs*x*-micro** was clarified first. Here those of **Cs2.5-micro** and **Cs2.5-bimodal** will be described as examples. During the preparation of **Cs2.5-micro**, the addition of Cs_2CO_3 solution to $H_4SiW_{12}O_{40}$

solution caused a white solid to precipitate from the milky suspension (Scheme 1). To obtain **Cs2.5-micro**, water was removed from the milky suspension by evaporation. To investigate the structure and composition of the precipitate and milky solution separately, the precipitate was removed by filtration, and the resulting milky solution was evaporated to form a solid (Scheme 1). The precipitate and solid obtained by evaporation of the milky solution are denoted as **Cs2.5(precipitate)** and **Cs2.5(solution)**, respectively. The mass ratio of **Cs2.5(precipitate)** to **Cs2.5(solution)** was 59/41. The Cs/polyanion ratio of **Cs2.5(precipitate)** was 3.7, which is much larger than 2.5. In the XRD pattern for **Cs2.5(precipitate)**, peaks consistent with phase C were observed, giving a Type I isotherm of N_2 adsorption-desorption (Figure 8a), which were the same as those for **Cs3.5-micro** and **Cs4.0-micro**. In addition, **Cs2.5(precipitate)** did not dissolve in ethanol at all, and the XRD pattern and N_2 adsorption-desorption isotherm were the same after the treatment in refluxing ethanol (Figures 8b)). The size of the crystallites of **Cs2.5(precipitate)** calculated from Scherrer's equation was 39 nm. From these results, we conclude that **Cs2.5(precipitate)** is microporous crystallites of $Cs_{3.7}H_{0.3}[SiW_{12}O_{40}]$ with 39 nm in size. On the other hand, Cs/polyanion ratio of **Cs2.5(solution)** was 1.0 and thus **Cs2.5(solution)** contained a small amount of Cs^+ and from XRD, it was confirmed to be a mixture of phase A ($H_4[SiW_{12}O_{40}]$) and phase B (Figure 8c). The amount of N_2 uptake for **Cs2.5(solution)** was

small (Figure 8c), and no micropores or mesopores were present. Upon treating **Cs2.5(solution)** in refluxing ethanol, 53% of the material dissolved, and the Cs/polyanion ratio became 2.2. Only the XRD pattern for phase B with a crystallite size of 23 nm (Figure 8d) was observed for the treated **Cs2.5(solution)**, meaning that phase A ($H_4[SiW_{12}O_{40}]$) was completely eliminated. The resulting solid gave a N_2 adsorption-desorption isotherm of type II (Figure 8d), which was dissimilar to that for **Cs2.5-bimoidal**. These results indicate that phase B is $Cs_{2.2}H_{1.8}[SiW_{12}O_{40}]$ with 23 nm in size and that it does not have any micropores.

From these results, we proposed the model shown in Scheme 2. **Cs2.5-micro** contained three crystallites with different *x* and crystallite sizes: $H_4[SiW_{12}O_{40}]$, $Cs_{2.2}H_{1.8}[SiW_{12}O_{40}]$(23 nm), and $Cs_{3.7}H_{0.3}[SiW_{12}O_{40}]$(39 nm), which correspond to phases A, B, and C, respectively. During the titration process for preparing **Cs2.5-micro**, $Cs_{3.7}H_{0.3}[SiW_{12}O_{40}]$(39 nm) precipitates first. In the milky supernatant, fine particles of $Cs_{2.2}H_{1.8}[SiW_{12}O_{40}]$(23 nm) are suspended, and $H_4[SiW_{12}O_{40}]$ dissolves. By evaporating the suspension, the fine particles of $Cs_{2.2}H_{1.8}[SiW_{12}O_{40}]$(23 nm) become physically mixed with those of $Cs_{3.7}H_{0.3}[SiW_{12}O_{40}]$(39 nm), and the interstitial voids between the crystallites are finally filled with $H_4[SiW_{12}O_{40}]$ as a glue to form the secondary particles (Figure 7(a)). When **Cs2.5-micro** is treated in ethanol, $H_4[SiW_{12}O_{40}]$ dissolves, forming interstitial voids at those sites. The interstitial voids

are the mesopores in **Cs2.5-bimodal**.

The presence of three crystallites in the appropriate ratio is crucial for the formation of the mesopores with regular shapes in **Cs*x*-bimodal**. When $H_4[SiW_{12}O_{40}]$ and $Cs_{2.2}H_{1.8}[SiW_{12}O_{40}]$(23 nm) are absent, as in the cases of **Cs3.5-micro** and **Cs4.0-micro**, no mesopores form because **Cs*x*-micro** contains only insoluble $Cs_{3.7}H_{0.3}[SiW_{12}O_{40}]$(39 nm). On the other hand, when a large amount of $H_4[SiW_{12}O_{40}]$ is present in **Cs*x*-micro**, as in the case of **Cs1.0-micro**, mesopores with wide distributions of sizes form because the shapes and sizes of the voids formed between the insoluble crystallites are irregular. In addition, the choice of solvent used for the treatment is another factor controlling the shape and volume of the mesopores. When water was used as a solvent for the treatment, mesopores with wide distributions of sizes formed (Figure S3). This is because not only $H_4[SiW_{12}O_{40}]$ but also a part of $Cs_{2.2}H_{1.8}[SiW_{12}O_{40}]$(23 nm) are soluble in water due to its high polarity. In contrast, the treatment of **Cs2.5-bimodal** in 1-propanol led to the formation of mesopores with small volumes due to the low solubility of $H_4[SiW_{12}O_{40}]$ (Figure S3).

During treatment of **Cs2.5-micro** in ethanol, $H_4[SiW_{12}O_{40}]$ dissolved, and thus, **Cs2.5-bimodal** consists of insoluble $Cs_{3.7}H_{0.3}[SiW_{12}O_{40}]$(39 nm) and $Cs_{2.2}H_{1.8}[SiW_{12}O_{40}]$(23 nm) crystallites. Since $Cs_{2.2}H_{1.8}[SiW_{12}O_{40}]$(23 nm) and $H_4[SiW_{12}O_{40}]$ have no micropores, **Micropore β** (0.62 nm) of

Cs2.5-micro and **Cs2.5-bimodal** (Figure 2) must be present in the crystal lattices of $Cs_{3.7}H_{0.3}[SiW_{12}O_{40}]$(39 nm). On the other hand, **Micropore α** (0.52 nm) appears to be interparticle voids formed mainly at the interface between the outer surface of $Cs_{3.7}H_{0.3}[SiW_{12}O_{40}]$(39 nm) and $H_4[SiW_{12}O_{40}]$ because **Micropore α** collapsed during the treatment in refluxing ethanol. However, further studies are needed.

3.3. Catalytic properties and post-treatment of **Cs2.5-bimodal** in sulfuric acid

Figure 9 shows catalytic activities of **Cs2.5-micro**, **Cs2.5-bimodal**, and **Cs2.5-bimodal(H_2SO_4)** towards the decomposition of isopropyl acetate (eq. 4) in *n*-decane at 373 K for 2 h.

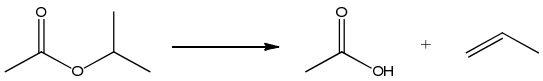

(eq. 4)

Cs2.5-bimodal(H_2SO_4) was obtained by post-treatment of **Cs2.5-bimodal** in sulfuric acid (see Experimental section 2.2.3). Treatment in ethanol decreased the catalytic activity; the catalytic activity of **Cs2.5-bimodal** was only one-third of that of **Cs2.5-micro**. The decrease in the catalytic activity is related to the dissolution of $H_4[SiW_{12}O_{40}]$ into ethanol, by which the mesopores were formed. In fact,

the acid amount for **Cs2.5-bimodal** estimated from NH_3-TPD (Figure 10) was 0.010 mmol g^{-1}, which is lower than that for **Cs2.5-micro** (0.099 mmol g^{-1}). In addition, the peak around 773 K, which corresponded to acidic protons, disappeared for **Cs2.5-bimodal**.

To increase the number of acid sites in **Cs2.5-bimodal**, **Cs2.5-bimodal** was treated in sulfuric acid to replace the Cs^+ ions on the surface with H^+. As shown in Figure 10, the peak due to acidic protons (773 K) partially recovered after post-treatment in sulfuric acid, and the acid amount of **Cs2.5-bimodal(H_2SO_4)** increased to 0.028 mmol g^{-1}. The crystalline structure of **Cs2.5-bimodal** was completely preserved during the post-treatment (Figure S4) and there was only little change in the surface areas by the post-treatment. The micropores were basically preserved during the post-treatment, which was confirmed from N_2 adsorption-desorption isotherms. Although the mesopores in **Cs2.5-bimodal** were preserved during the post-treatment, the mesopore volume slightly decreased (Figure S5). The exchange of Cs^+ with H^+ for **Cs2.5-bimodal(H_2SO_4)** was also confirmed by using elemental analysis. The Cs/polyanion ratio decreased from 2.9 (**Cs2.5-bimodal**) to 2.6 (**Cs2.5-bimodal(H_2SO_4)**). The catalytic activity of **Cs2.5-bimodal(H_2SO_4)** was about twice that of **Cs2.5-bimodal** (Figure 9). Since only negligible amounts of sulfur were detected in **Cs2.5-bimodal(H_2SO_4)** by using elemental analysis, it was not modified with sulfate ion, forming sulfated metal oxides, like sulfated zirconia.

Figure 11 shows time courses for the decomposition of isopropyl acetate over **Cs2.5-bimodal(H_2SO_4)** along with those after the catalyst was filtered off at 60 min. The conversion increased with reaction time, but the reaction completely stopped after the catalyst was filtered off from the reaction solution, indicating that **Cs2.5-bimodal(H_2SO_4)** acted as a heterogeneous catalyst.

One advantage of catalysts with mesopores is that they can be used in reactions involving large reactants and products, which are too big for microporous catalysts. To demonstrate the advantage of the mesoporosity and high acid strength of **Cs2.5-bimodal(H_2SO_4)**, we carried out the transesterification of glyceryl tributyrate with methanol (eq. 5) over various solid acids and compared their catalytic performances with that of **Cs2.5-bimodal(H_2SO_4)** (Figure 12).

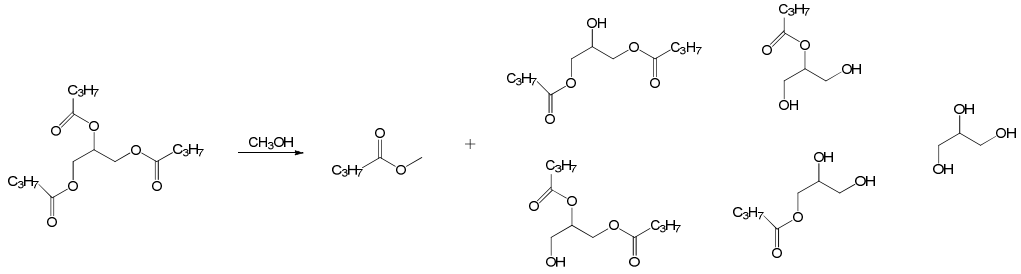

(eq.5)

Silica-alumina and zeolites, including H-Y, H-β, and H-ZSM-5, showed little or negligible activity due to their weak acid strengths and/or microporosity. Although fresh **Cs2.5-micro** showed the highest activity among the catalysts, its catalytic activity significantly decreased when it was reused. The high activity for the first run and low activity for the second run are due to dissolution of the acidic component of

Cs2.5-micro into the polar reaction solution, which was mainly composed of methanol during the first run. In separate experiment, it was confirmed that 14.9% of **Cs2.5-micro** was dissolved in methanol. In contrast to **Cs2.5-micro**, the recovered **Cs2.5-bimodal(H_2SO_4)** showed similar activity for the reaction to that of the fresh one. In other words, there was little catalyst deactivation. This was because dissolution of **Cs2.5-bimodal(H_2SO_4)** in methanol was only little (3.9%), which was basically the same as that of **Cs2.5-bimodal**.

Cs2.5-bimodal(H_2SO_4) had a greater activity than Amberlyst-15 did. Since Amberlyst-15 has a larger number of acid sites (4.7 mmol g^{-1}) than **Cs2.5-bimodal(H_2SO_4)** (0.028 mmol g^{-1}) does, the strong acid strength as well as mesoporosity of **Cs2.5-bimodal(H_2SO_4)** greatly contributes to the high activity towards the transesterification of glyceryl tributyrate with methanol.

4. Conclusions

Treatment of microporous $Cs_xH_{4-x}SiW_{12}O_{40}$ (**Cs*x*-micro**) with x = 1.0–2.5 in refluxing ethanol resulted in the formation of mesopores in the particle with the preservation of the micropores. In particular, **Cs2.5-micro** transformed into a bimodal Cs salt (**Cs2.5-bimodal**) with a narrow distribution of mesopore diameters (3.7 nm) and large mesopore volumes. **Cs2.5-micro** was composed of three

microcrystallites ($Cs_{3.7}H_{0.3}[SiW_{12}O_{40}]$ with an average crystallite size of 39 nm, $Cs_{2.2}H_{1.7}[SiW_{12}O_{40}]$ with an average crystallite size of 23 nm, and $H_4[SiW_{12}O_{40}]$), and these aggregated to form secondary particles. Treating **Cs2.5-micro** in ethanol caused part of the microcrystallites, mainly $H_4[SiW_{12}O_{40}]$, to dissolve, creating voids between the insoluble parts, where the $H_4[SiW_{12}O_{40}]$ crystallites were. These interstitial voids were the mesopores in **Cs2.5-bimodal**.

The catalytic activity of bimodal **Cs2.5-bimodal** towards the decomposition of isopropyl acetate in the liquid phase was only one-third of that of untreated microporous **Cs2.5-micro** because the acidic component, mainly $H_4[SiW_{12}O_{40}]$, was eliminated from the solid at the time that the mesopores formed during the treatment. Further thermal treatment of **Cs2.5-bimodal** in sulfuric acid led to a threefold increase in the acid amount due to the substitution of Cs^+ ions on the surface with H^+ ions, and thus, the catalytic activity for the decomposition of isopropyl acetate increased. **Cs2.5-bimodal** treated with sulfuric acid showed high activity towards the transesterification of bulky glyceryl tributyrate with methanol due to its strong acid strength and mesoporosity.

Acknowledgement

This work was supported by KAKENHI (24760634).

References

[1] D.P. Serrano, J. Aguado, J.M. Escola, ACS Catal. 2 (2012) 1924-1941.

[2] D.O. de Zárate, F. Bouyer, H. Zschiedrich, P.J. Kooyman, P. Trens, J. Iapichella, R. Durand, C. Guillem, E. Prouzet, Chem. Mater. 20 (2008) 1410-1420.

[3] M. Enterría, F. Suírez-García, A. Martínez-Alonso, J.M.D. Tascón, J. Alloys Comp. 589 (2014) 60-69.

[4] C.R. Patil, P.S. Niphadkar, V.V. Bolade, P.N. Joshi, Catal. Commun. 43 (2014) 188-191.

[5] J. Ding, H. Liu, P. Yuan, G. Shi, X. Bao, ChemCatChem 5 (2013) 2258-2269.

[6] Y. Yue, Z.-A. Qiao, P.F. Fulvio, A.J. Binder, C. Tian, J. Chen, K.M. Nelson, X. Zhu, S. Dai. J. Am. Chem. Soc. 135 (2013) 9572-9575.

[7] L.G. Possato, R.N. Diniz, T. Garetto, S.H. Pulcinelli, C.V. Santilli, L. Martins, J. Catal. 300 (2013) 102-112.

[8] Y.H. Kim, K.H. Lee, C.-M. Nam, J.S. Lee, ChemCatChem 4 (2012) 1143-1153.

[9] S. Schlienger, J. Alauzun, F. Michaux, L. Vidal, J. Parmentier, C. Gervais, F. Babonneau, S. Bernard, P.

Miele, J.B. Parra, Chem. Mater. 24 (2012) 88-96.

[10] X.-Y, Yang, G. Tian, L.-H. Chen, Y. Li, J.C. Rooke, Y.-X. Wei, Z.-M. Liu, Z. Deng, G.V. Tendeloo, B.-L. Su, Chem. Eur. J. 17 (2011) 14987-14995.

[11] X. Zhang, K. Tao, T. Kubota, T. Shimamura, T. Kawabata, K. Matsuda, S. Ikeno, N. Tsubaki, Appl. Catal. A 405 (2011) 160-165.

[12] N. Danilina, S.A. Castelanelli, E. Troussard, J.A. van Bokhoven, Catal. Today 168 (2011) 80-85.

[13] D.P. Serrano, R. Sanz, P. Pizarro, I. Moreno, Top. Catal. 53 (2010) 1319-1329.

[14] N. Danilina, F. Krumeich, J.A van Bokhoven, J. Catal. 272 (2010) 37-43.

[15] K.M. Jinka, H.C. Bajaj, R.V. Jasra, E.A. Prasetyanto, S.-E. Park, Top. Catal. 53 (2010) 238-246.

[16] C. Perego, R. Millini, Chem. Soc. Rev. 42 (2013) 3956-3976.

[17] M. Rutkowska, L. Chmielarz, D. Macina, Z. Piwowarska, B. Dudek, A. Adamski, S. Witkowski, Z. Sojka, L. Obalová, C.J. Van Oers, P. Cool, Appl. Catal. B 146 (2014) 112-122.

[18] F.L. Bleken, K. Barbera, F. Bonino, U. Olsbye, K.P. Lillerud, S. Bordiga, P. Beatp, T.V.W. Janssens, S. Svelle, J. Catal. 307 (2013) 62-73.

[19] L. Wu, V. Degirmenci, P.C.M.M. Magusin, N.J.H.G.M. Lousberg, E.J.M. Hensen, J. Catal. 298 (2013) 27-40.

[20] H. Mochizuki, T. Yokoi, H. Imai, S. Namba, J.N. Kondo, T. Tatsumi, Appl. Catal. A 449 (2012) 188-197.

[21] Y. Fang, H. Hu, J. Am. Chem. Soc. 128 (2006) 10636-10637.

[22] M. Choi, H.S. Cho, R. Srivastava, C. Venkatesan, D.-H. Choi, R. Ryoo, Nature Mat. 5 (2006) 718-723.

[23] L. Schmidt, A. Boisen, E. Gustavsson, K. Ståhl, S. Pehrson, S. Dahl, A. Carlsson, C.J.H. Jacobsen, Chem. Mater. 13 (2001) 4416-4418.

[24] Y. Tao, H. Kanoh, K. Kaneko, J. Am. Chem. Soc. 125 (2003) 6044-6045.

[25] A.H. Janssen, I. Schmidt, C.J.H. Jacobsen, A.J. Koster, K.P. de Jong, Micropore Mesopore Mater. 65 (2003) 59-75.

[26] M. Ogura, S. Shinomiya, J. Tateno, Y. Nara, E. Kikuchi, M. Matsukata, Chem. Lett. (2000) 882-883.

[27] M. Ogura, S. Shinomiya, J. Tateno, Y. Nara, M. Nomura, E. Kikuchi, M. Matsukata, Appl. Catal. A 219 (2001) 33-43.

[28] J.C. Groen, J.C. Jansen, J.A. Moulijn, J. Pérez-Ramírez, J. Phys. Chem. B 108 (2004) 13062-13065.

[29] T. Suzuki, T. Okuhara, Micropore Mesopore Mater. 43 (2001) 83-89.

[30] M. Ogura, Top. Catal. 12 (2008) 16-27.

[31] T. Okuhara, N. Mizuno, M. Misono, Adv. Catal. 41 (1996) 113–252.

[32] M.T. Pope, “Heteropoly and Isopoly Oxometalates” Springer-Verlag, Berlin, 1983.

[33] I.V. Kozhevnikov, Chem. Rev. 98 (1998) 171-198.

[34] T. Okuhara, T. Nishimura, H. Watanabe, M. Misono, J. Mol. Catal. 74 (1992) 247-256.

[35] T. Okuhara, T. Nishimura, M. Misono, Stud. Surf. Sci. Catal. 101 (1996) 581-590.

[36] M. Misono, N. Mizuno, K. Katamura, A. Kasai, Y. Konishi, K. Sakata, T. Okuhara, Y. Yoneda, Bull. Chem. Soc. Jpn. 55 (1982) 400-406.

[37] L.C. Jozefowicz, H.G. Karge, E. Vasilyeva, J.M. Moffat, Microporous Mater. 1 (1993) 313-322.

[38] F. Lefebvre, F.X. Liu-Cai, A. Auroux, J. Mater. Chem. 4 (1994) 125-131.

[39] D.J. Parrollo, C. Lee, R.J. Gorte, D. White, W.E. Farneth, J. Phys. Chem. 99 (1995) 8745-8749.

[40] A. Zheng, S.-J. Huang, S.-B. Liu, F. Deng, Phys. Chem. Chem. Phys. 13 (2011) 14889-14901.

[41] N. Feng, A, Zheng, S.-J. Huang, H. Zhang, N. Yu, C.-Y. Yang, S.-B. Liu, F. Deng. J. Phys. Chem. C. 114 (2010) 15464-15472.

[42] M. Misono, Catal. Rev. -Sci. Eng. 29 (1987) 269-321.

[43] J.B. McMonagle, J.B. Moffat. J. Colloid Interface Sci. 101 (1984) 479-488.

[44] T. Okuhara, T. Nishimura, M. Misono, Chem. Lett. (1995) 155-156.

[45] Y. Kamiya, S. Sano, Y. Miura, Y. Uchida, Y. Ogawa, Y. Iwase, T. Okuhara, Chem. Lett. 39 (2010) 881-883.

[46] I.V. Kozhevnikov, Catal. Rev.-Sci. Eng. 37 (1995) 311-352.

[47] T. Yamada, Y. Yoshinaga, T. Okuhara, Bull. Chem. Soc. Jpn. 71 (1998) 2727-2734.

[48] T. Yamada, K. Johkan, T. Okuhara, Micropore Mesopore Mater. 26 (1998) 109-115.

[49] Y. Yoshinaga, K. Seki, T. Nakato, T. Okuhara, Angew. Chem. Int. Ed. 36 (1997) 2833-2835.

[50] T. Okuhara, H. Watanabe, T. Nishimura, K. Inumaru, M. Misono, Chem. Mater. 12 (2000) 2230-2238.

[51] Y. Yoshinaga, T. Suzuki, M. Yoshimune, T. Okuhara, Top. Catal. 19 (2002) 179-185.

[52] T. Okuhara, T. Nakato, Catal. Surv. Jpn. 2 (1998) 31-44.

[53] T. Okuhara. Chem. Rev. 102 (2002) 3641-3666.

[54] T. Okuhara, N. Mizuno, M. Misono, Appl. Catal. A 222 (2001) 63-77.

[55] Y. Miura, H. Imai, T. Yokoi, T. Tatsumi, Y. Kamiya, Micropore Mesopore Mater. 174 (2013) 34-43.

[56] Y. Ogasawara, S. Uchida, T. Maruichi, R. Ishikawa, N. Shibata, Y. Ikugara, N. Mizuno, Chem. Mater. 25 (2013) 905-911.

[57] A. Saito, H.C. Foley, Microporous Mater. 3 (1995) 531-542.

[58] V.B. Fenelonov, V.N. Romannikov, A.Y. Derevyankin, Micropore Mesopore Mater. 28 (1999) 57-72.

Figure Captions

Figure 1 N_2 adsorption-desorption isotherms at 77 K for **Cs*x*-micro** and **Cs*x*-bimodal**. x = (a) 1.0, (b) 1.5, (c) 2.0, (d) 2.5, (e) 3.0, (f) 3.5, and (g) 4.0. Circle: **Cs*x*-micro**, and square: **Cs*x*-bimodal**. Filled symbol: adsorption branch, and open symbol: desorption branch.

Figure 2 Micropore and mesopore size distributions in **Cs2.5-micro** (solid line) and **Cs2.5-bimodal** (dashed line).

Figure 3 Dependence of mesopore volumes on the Cs content (x) before and after the treatment in ethanol. (○) **Cs*x*-micro** and (●) **Cs*x*-bimodal**.

Figure 4 Relationship between the dissolution rate of **Cs*x*-micro** treated in ethanol and Cs content (x). Treatment conditions: **Cs*x*-micro**, 2 g; volume of ethanol, 30 cm^3; temperature, 347 K; time, 4 h. After treatment, the remaining solid was collected on a membrane filter, washed with ethanol, dried in air, and weighted.

Figure 5 Cs/polyanion (= Cs/12W) ratio in (○) **Cs*x*-micro** and (●) **Cs*x*-bimodal**. The dashed line represents Cs/polyanion = *x*.

Figure 6 XRD patterns of (A) **Cs*x*-micro** and (B) **Cs*x*-bimodal**.

Figure 7 SEM images of (a) **Cs2.5-micro** and (b) **Cs2.5-bimodal**.

Figure 8 XRD patterns and N_2 adsorption-desorption isotherms for **Cs2.5(precipitate)** and **Cs2.5(solution)** and for the materials obtained after treatment in ethanol. (a) **Cs2.5(precipitate)**, (b) material obtained after treatment of **Cs2.5(precipitate)** in ethanol, (c) **Cs2.5(solution)**, and (d) material obtained after treatment of **Cs2.5(solution)** in ethanol.

Figure 9 Results from catalytic decomposition of isopropyl acetate over **Cs2.5-micro**, **Cs2.5-bimodal**, and **Cs2.5-bimodal(H_2SO_4)**. Reaction conditions: isopropyl acetate, 8 mmol; *n*-decane (solvent), 28 cm^3; 1,3,5-triisopropyl benzene (internal standard), 4 mmol; catalyst weight, 0.1 g; reaction temperature, 373 K; reaction time 2 h.

Figure 10 Ammonia-TPD profiles of (a) **Cs2.5-micro**, (b) **Cs2.5-bimodal**, and (c) **Cs2.5-bimodal(H_2SO_4)**.

Figure 11 Time courses for decomposition of isopropyl acetate over **Cs2.5-bimodal(H_2SO_4)** with the catalyst (●) present during the entire reaction and (○) after it was removed from the reaction solution at 60 min. Reaction conditions: isopropyl acetate, 8 mmol; *n*-decane (solvent), 28 cm^3; 1,3,5-triisopropyl benzene (internal standard), 4 mmol; catalyst weight 0.1 g, and reaction temperature 373 K.

Figure 12 Results from the catalytic transesterification of glyceryl tributyrate with methanol over solid acid catalysts. Reaction conditions: glyceryl tributyrate, 10 mmol; methanol, 9.6 g (300 mmol); n-hexyl ether (internal standard), 2.5 mmol; catalyst weight, 0.2 g; reaction temperature, 333 K; reaction time, 24 h. For **Cs2.5-micro** and **Cs2.5-bimodal(H_2SO_4)**, their reusabilities were checked. After the first run, the catalyst was separated by centrifugation and dried at 373 K.

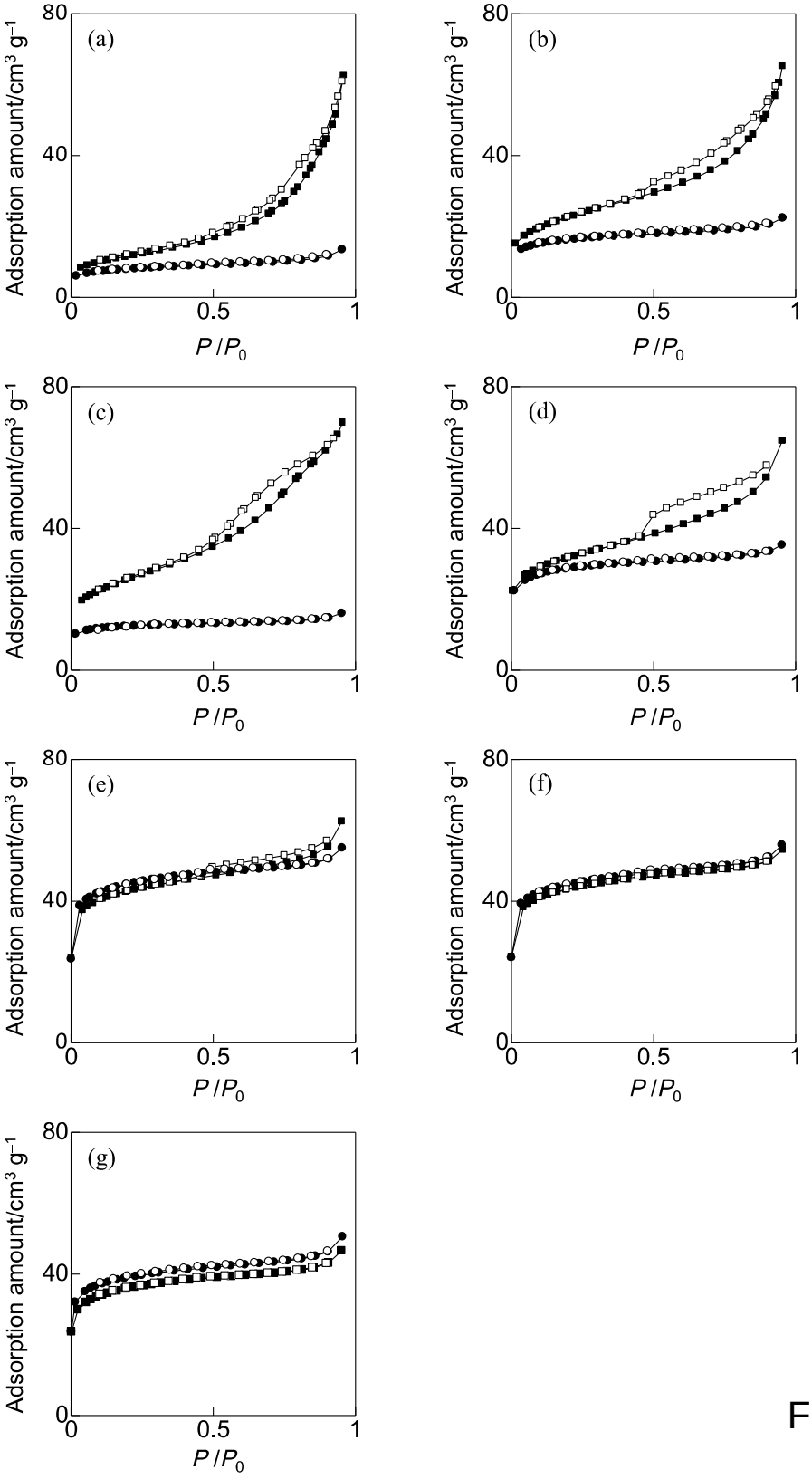

Fig. 1

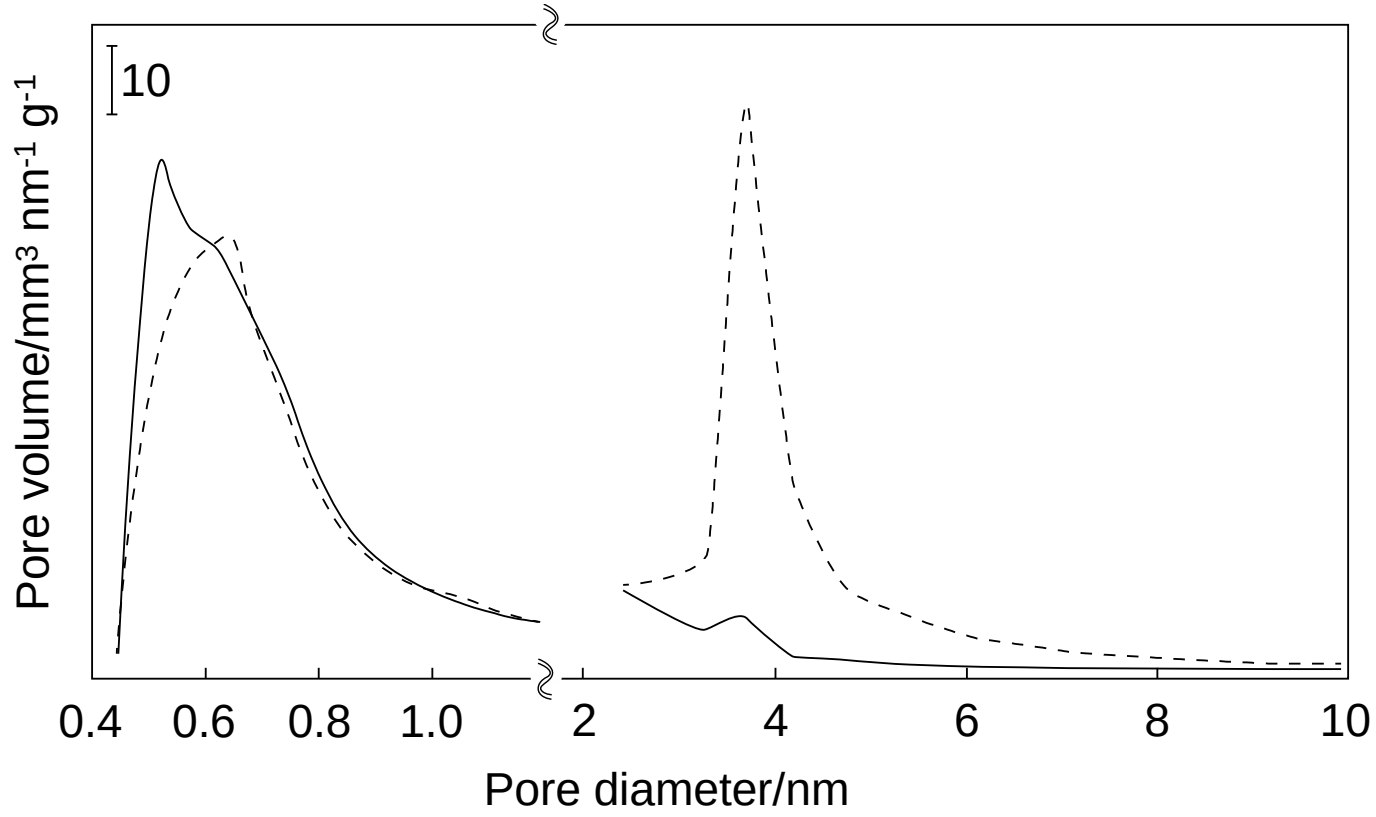

Fig. 2

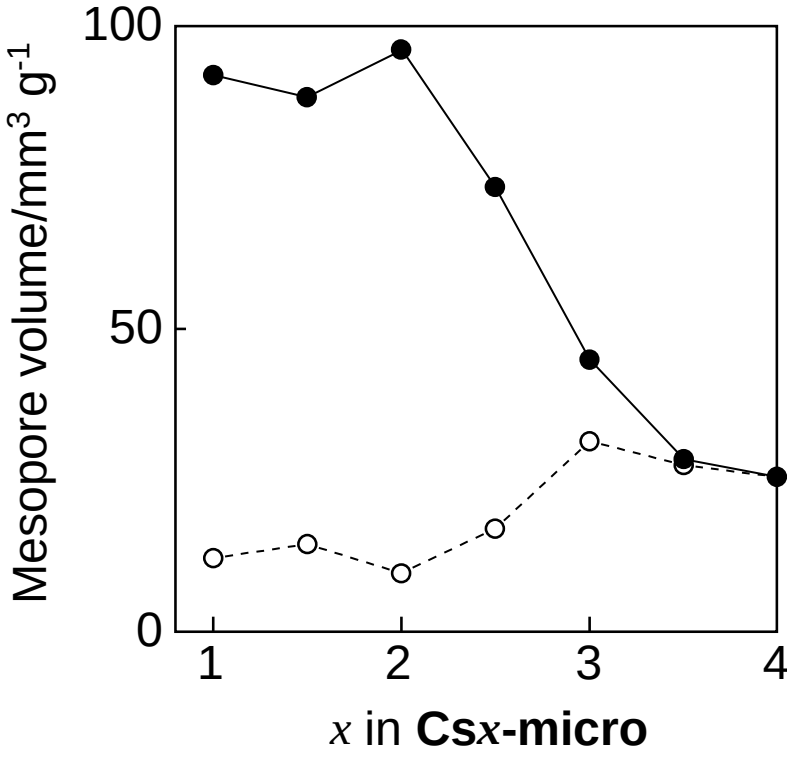

Fig. 3

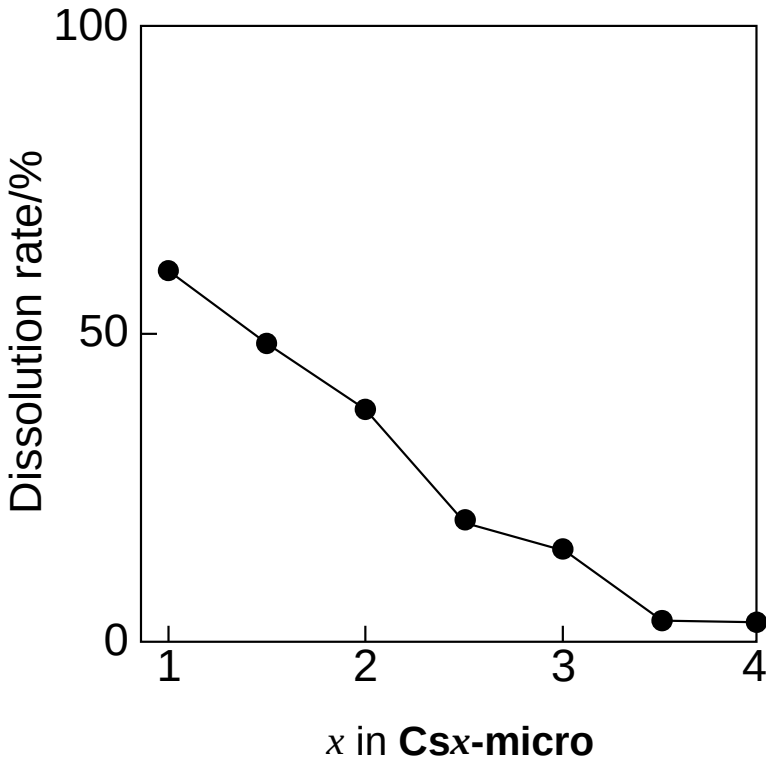

Fig. 4

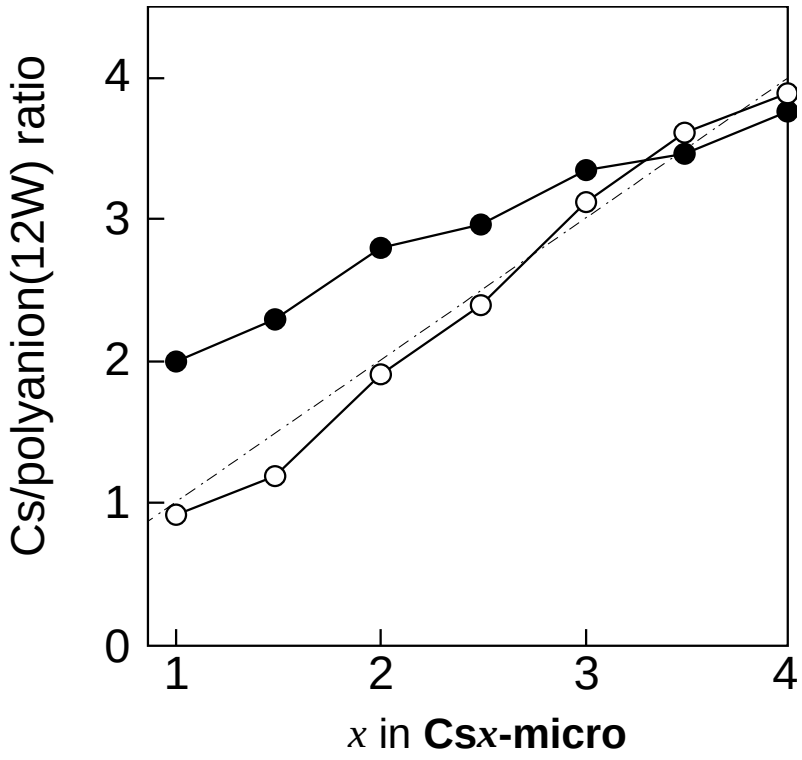

Fig. 5

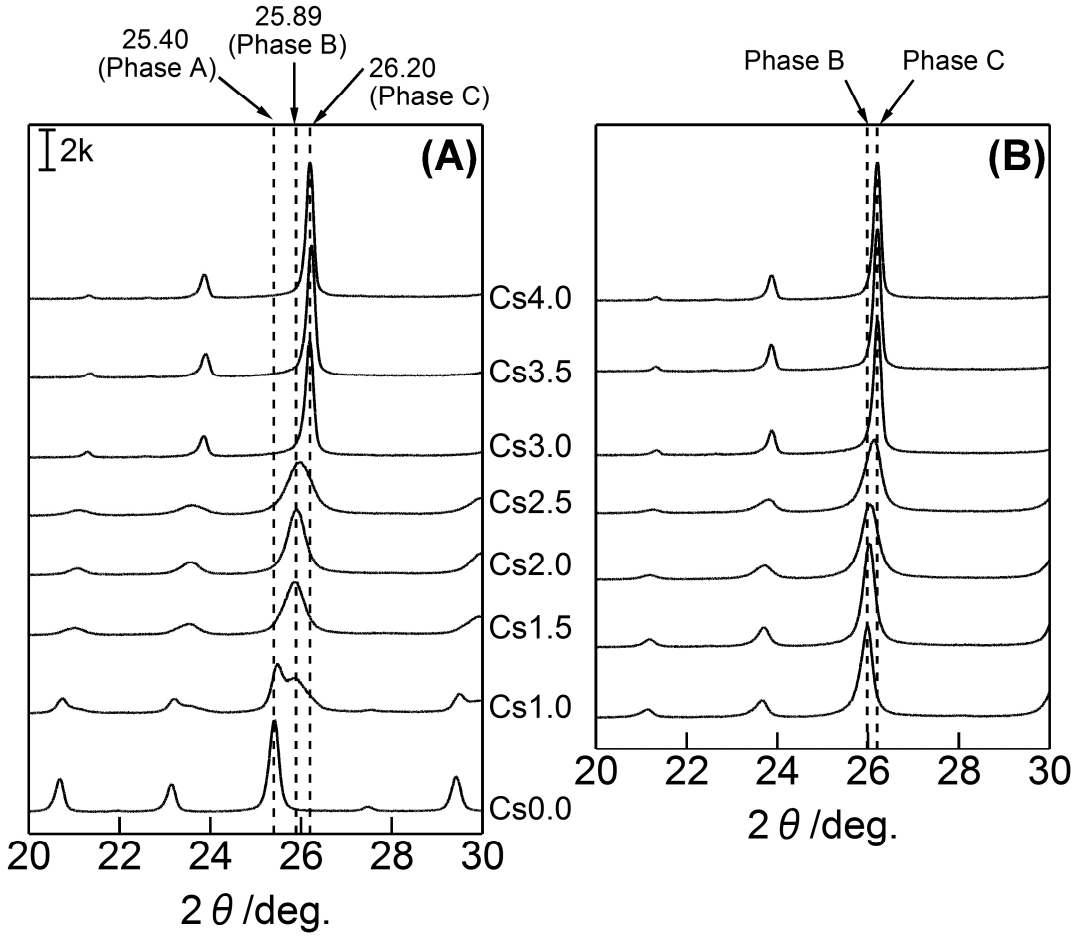
25.40
(Phase A)
25.89
(Phase B)
26.20
(Phase C)
2k
(A)
Cs4.0
Cs3.5
Cs3.0
Cs2.5
Cs2.0
Cs1.5
Cs1.0
Cs0.0
20
22
24
26
28
30
2θ /deg.
Phase B
Phase C
(B)
20
22
24
26
28
30
2θ /deg.

Fig. 6

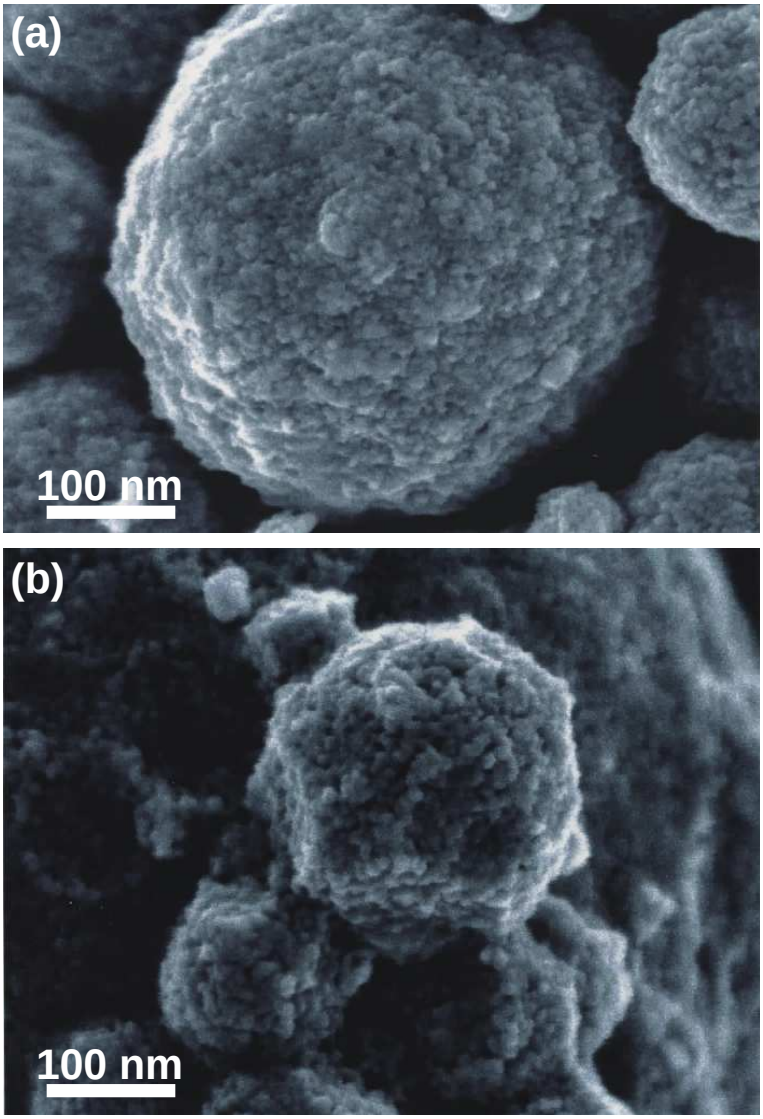

Fig. 7

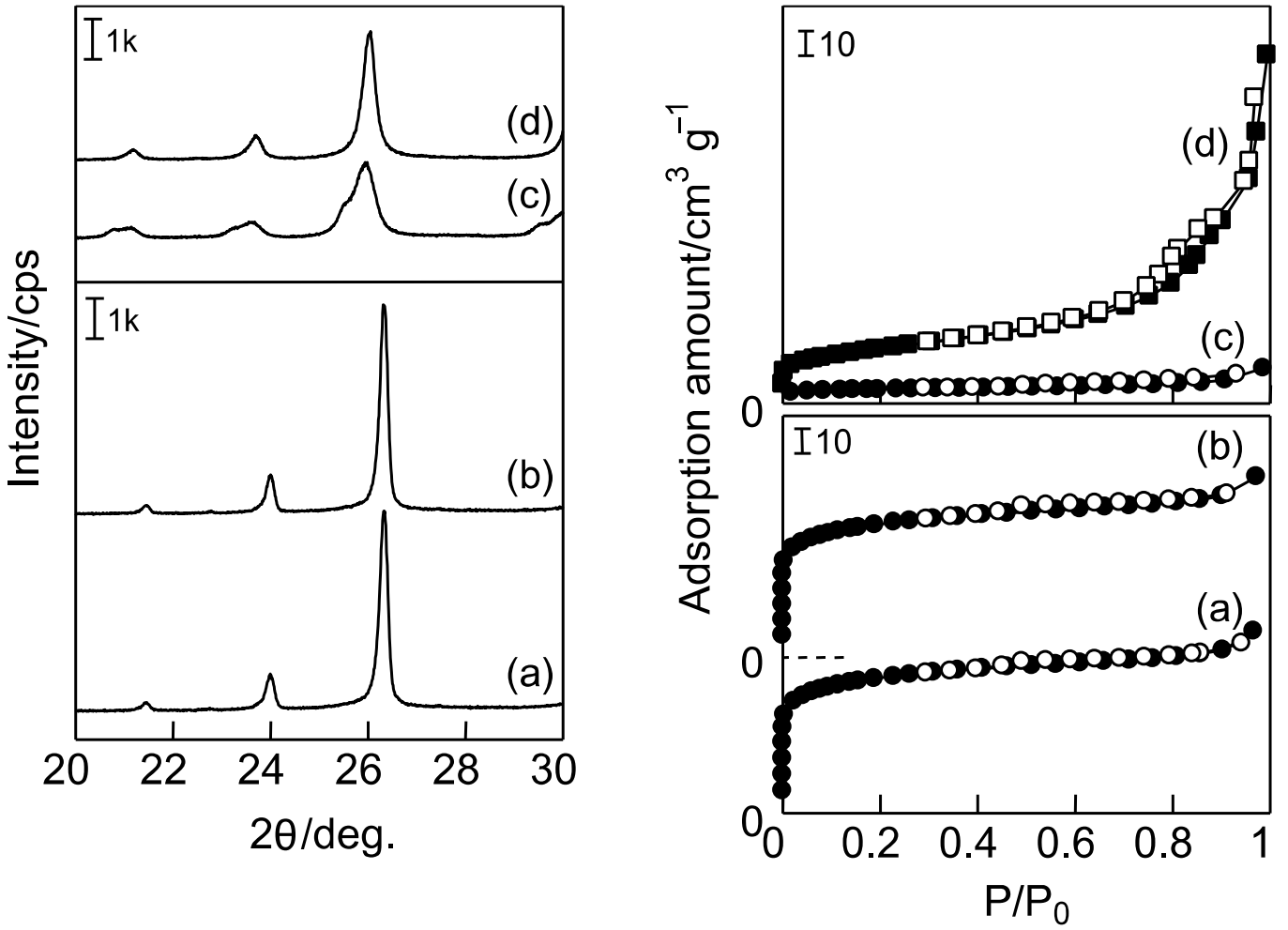
1k
(d)
(c)
1k
(b)
(a)
Intensity/cps
20
22
24
26
28
30
2θ/deg.
I10
(d)
(c)
0
I10
(b)
(a)
0
0
0
0.2
0.4
0.6
0.8
1
P/P0
Adsorption amount/cm3 g-1

Fig. 8

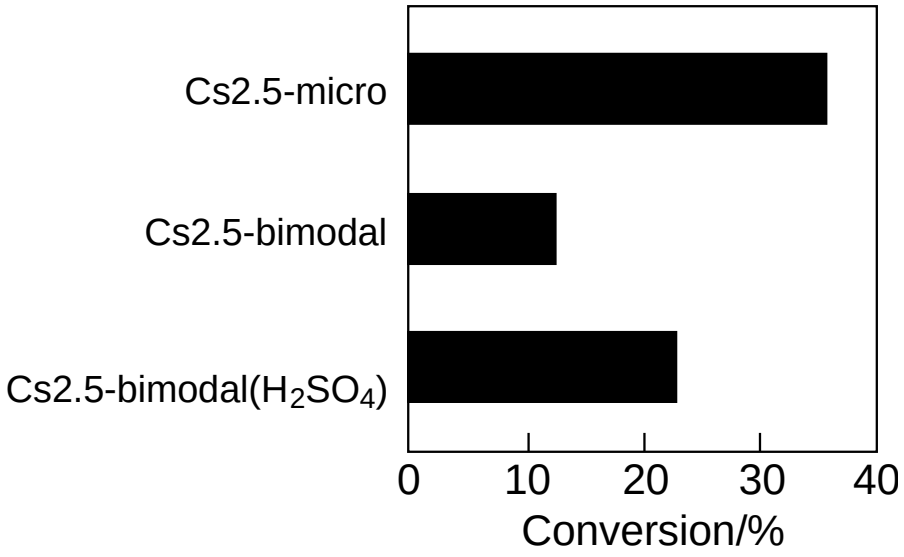
Cs2.5-micro
Cs2.5-bimodal
Cs2.5-bimodal(H_2SO_4)
0
10
20
30
40
Conversion/%

Fig. 9

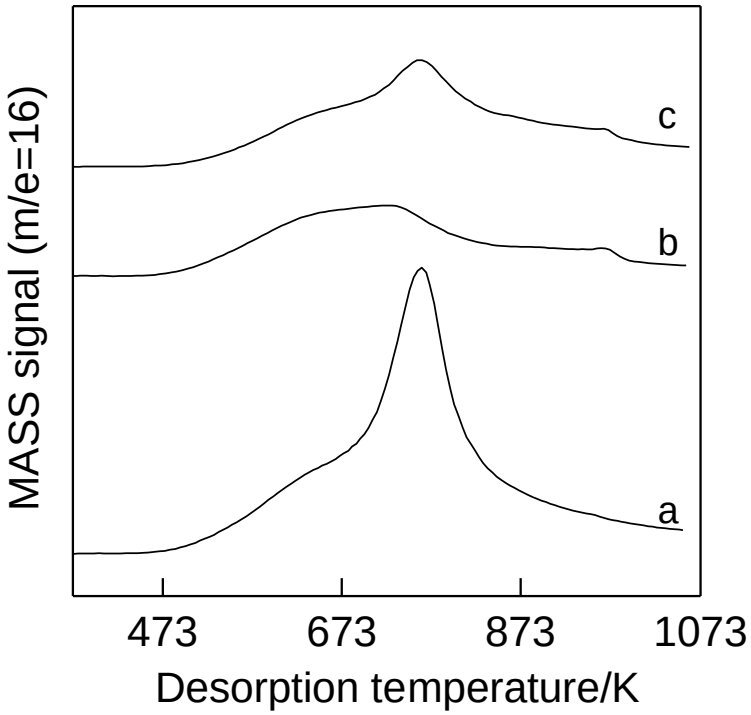
MASS signal (m/e=16)
c
b
a
473
673
873
1073
Desorption temperature/K

Fig. 10

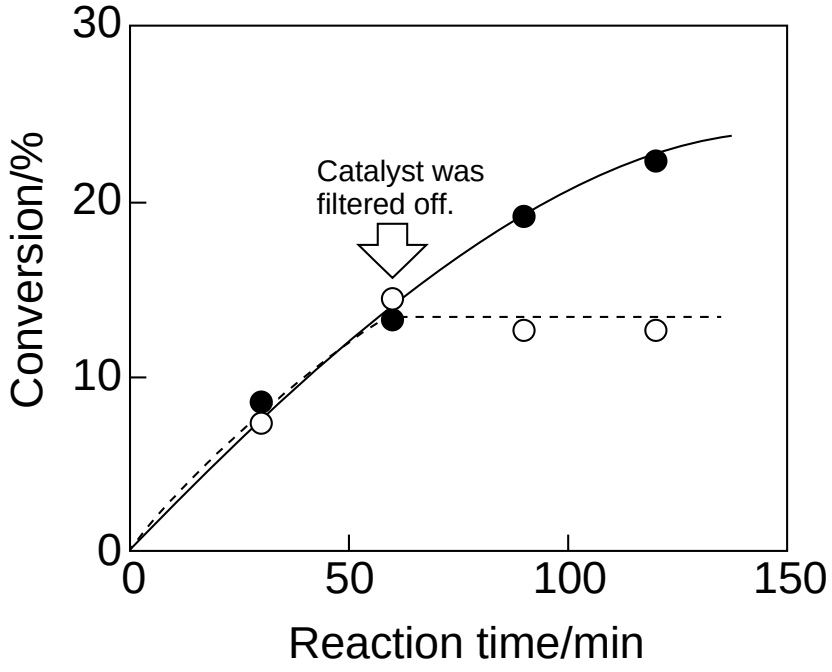
30
20
10
0
Conversion/%
Catalyst was
filtered off.
0
50
100
150
Reaction time/min

Fig. 11

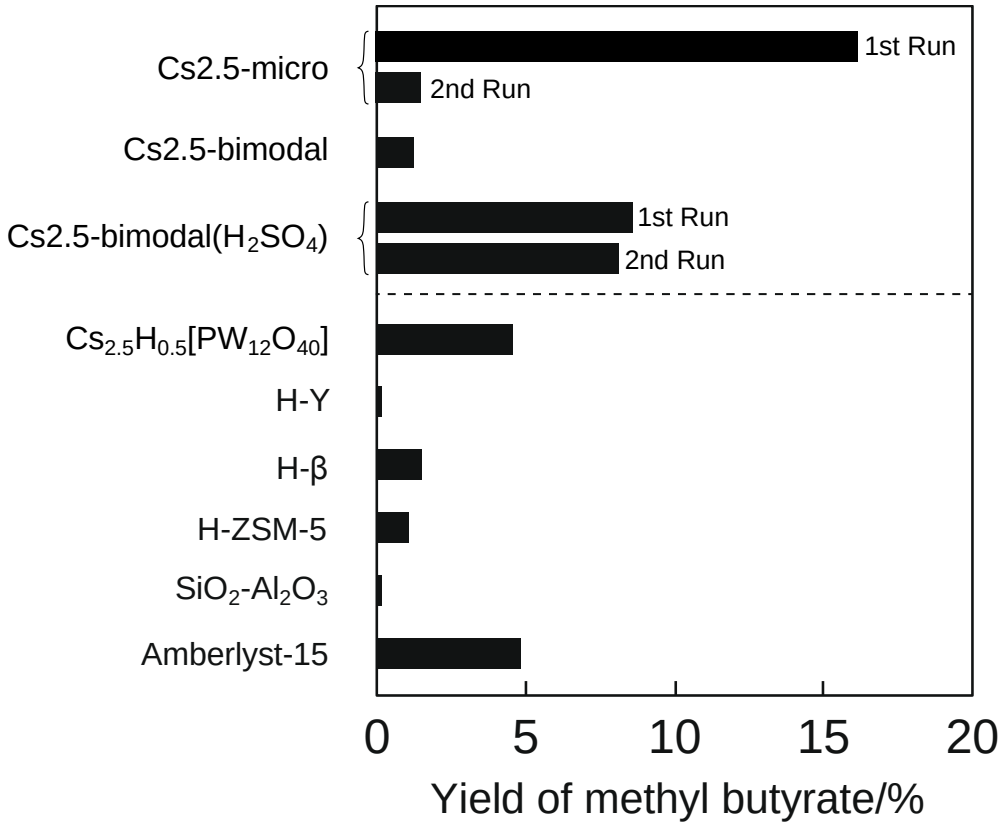
Cs2.5-micro
1st Run
2nd Run
Cs2.5-bimodal
Cs2.5-bimodal(H2SO4)
1st Run
2nd Run
Cs2.5H0.5[PW12O40]
H-Y
H-β
H-ZSM-5
SiO2-Al2O3
Amberlyst-15
0
5
10
15
20
Yield of methyl butyrate/%

Fig. 12

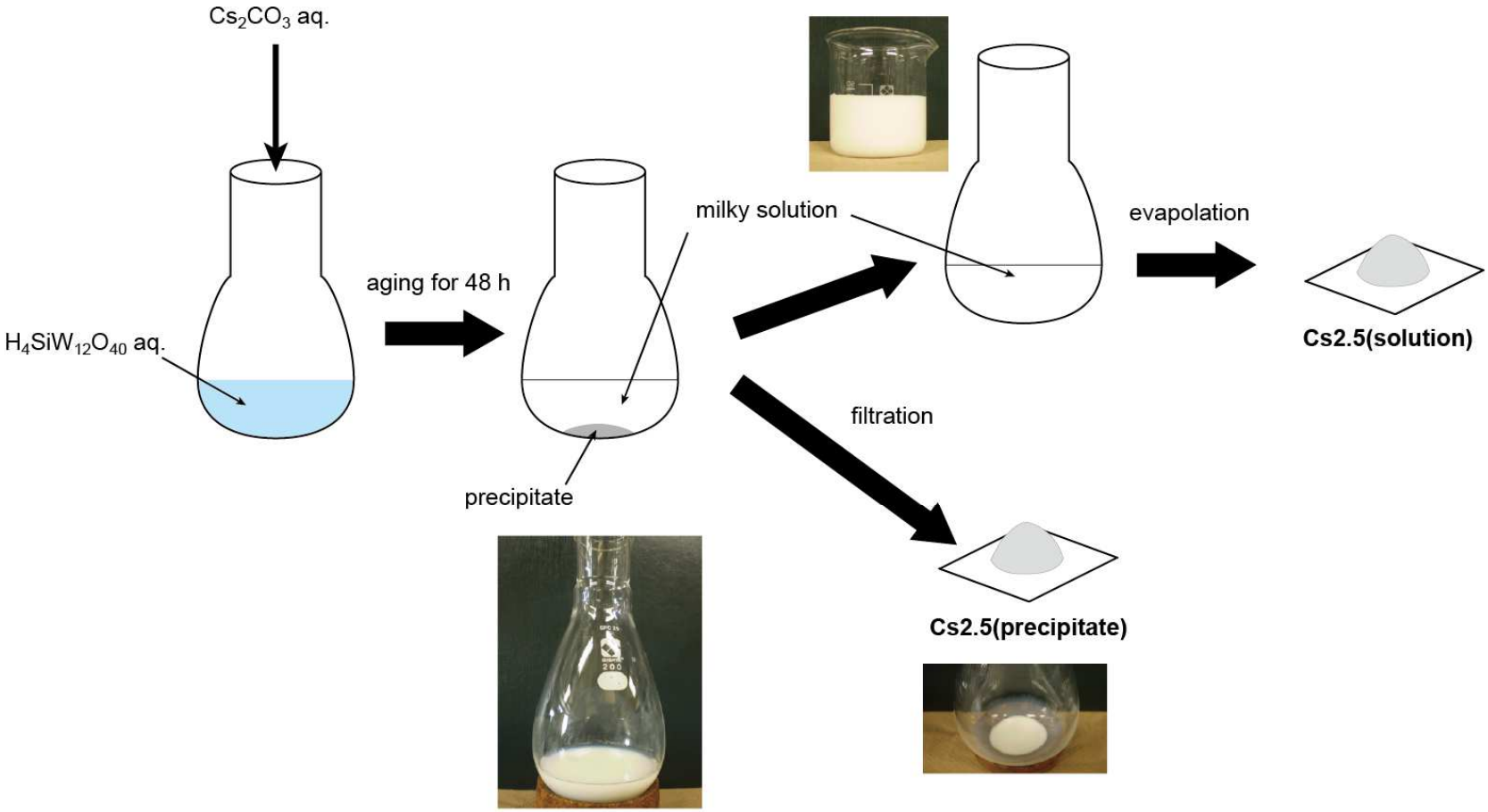
Cs_2CO_3 aq.
$H_4SiW_{12}O_{40}$ aq.
aging for 48 h
precipitate
milky solution
filtration
evapolation
Cs2.5(solution)
Cs2.5(precipitate)

Scheme 1

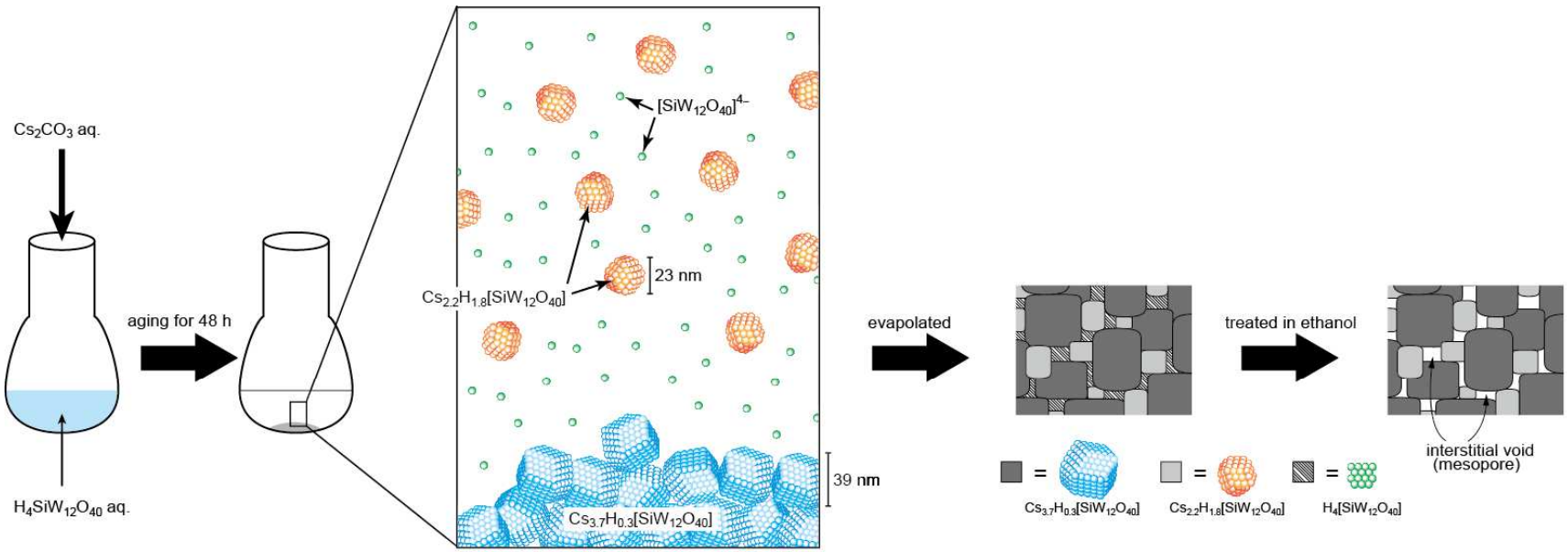
Cs_2CO_3 aq.
$H_4SiW_{12}O_{40}$ aq.
aging for 48 h
$[SiW_{12}O_{40}]^{4-}$
$Cs_{2.2}H_{1.8}[SiW_{12}O_{40}]$
23 nm
39 nm
$Cs_{3.7}H_{0.3}[SiW_{12}O_{40}]$
evapolated
treated in ethanol
interstitial void
(mesopore)
=
=
=
$Cs_{3.7}H_{0.3}[SiW_{12}O_{40}]$
$Cs_{2.2}H_{1.8}[SiW_{12}O_{40}]$
$H_4[SiW_{12}O_{40}]$

Scheme 2